The American Journal of Human Genetics

Supplemental Data

Mutations in *CLPB* Cause Intellectual Disability, Congenital Neutropenia, Progressive Brain Atrophy, Movement Disorder, Cataracts, and 3-Methylglutaconic Aciduria

Saskia B. Wortmann, Szymon Ziętkiewicz, Maria Kousi, Radek Szklarczyk, Tobias B. Haack, Søren W. Gersting, Ania C. Muntau, Aleksandar Rakovic, G. Herma Renkema, Richard J. Rodenburg, Tim M. Strom, Thomas Meitinger, M. Estela Rubio-Gozalbo, Elzbieta Chrusciel, Felix Distelmaier, Christelle Golzio, Joop H. Jansen, Clara van Karnebeek, Yolanda Lillquist, Thomas Lücke, Katrin Õunap, Riina Zordania, Joy Yaplito-Lee, Hans van Bokhoven, Johannes N. Spelbrink, Frédéric M. Vaz, Mia Pras-Raves, Rafal Ploski, Ewa Pronicka, Christine Klein, Michel A.A.P. Willemsen, Arjan P.M. de Brouwer, Holger Prokisch, Nicholas Katsanis, and Ron A. Wevers

Supplemental information

Supplemental case reports

1. Mild phenotype (cataracts, neutropenia, no ID/DD, no movement disorder, no MRI abnormalities)

Individual 1 came to medical attention at 18 months of age with fever and skin infection requiring antibiotics. Severe neutropenia (0.1 G/L) was noted. His neutrophil counts varied (0.1 – 1.1 G/L) in the further course, but he never experienced any infections nor required antibiotics since then. When his younger sister, **individual 2,** was born with bilateral nuclear cataracts, and also showed neutropenia (0.7 G/L) both individuals were evaluated further. Their development and growth until the age of 10 and eight years, respectively, is normal. Both recently had an extensive psychological examination including an IQ assessment, which yielded scores in the average range. The brother was further diagnosed with attention deficit hyperactivity disorder (ADHD), dyslexia and dysgraphia and the sister with a tendency to impulsivity. Though no radiological data are available for individual 1, the MRI of individual 2 at the age of eight years was normal.

2. Moderate phenotype (cataracts, neutropenia, infections, congenital hypotonia progressing to spasticity, mild to severe ID/DD, movement disorder, increasing severity of MRI abnormalities)

Individual 3 presented with intra-uterine growth restriction (IUGR) but showed catch up growth to birth weight p10, length p50, head circumference p3. Bilateral talipes were noted on prenatal ultrasound. The newborn period was complicated by generalized hypotonia, feeding difficulties, and one episode of hypoglycaemia. He underwent serial casting and an achilles tenotomy for talipes. He has intermittent left esotropia and amblyopia with normal fundi, but no cataracts. Since the age of ten months he had recurrent episodes of neutropenia (0.04 G/L) in the context of febrile illnesses but has responded well to short courses of G-CSF. His development is globally delayed. Currently, at the age of 5 years nine months, he has mild truncal hypotonia, is able to walk independently but with a stooped posture and ataxic gait. He is able to spell his name and speak in simple sentences. He has short stature (p10) and microcephaly (p2). Echocardiography is normal.

The proband has a younger brother, **individual 4,** and sister, **individual 5** (uncomplicated twin pregnancy). The boy had generalized hypotonia, more prominent than his twin sister.

Both had problems with hypoglycaemia and poor feeding. At seven months of age, bilateral cataracts were detected in the male individual, which were removed surgically. Ophthalmological investigations in the girl were normal. At 18 months microcephaly became apparent in both children. Both affected individuals remain hypotonic and although they continue gaining skills, their development is globally delayed. At 21 months of age, they are able to sit independently and to crawl. They babble and are able to indicate what they want. Neither twin has had documented febrile neutropenic episodes to date. Echocardiography, hearing assessment and cranial ultrasound were normal.

Individual 6 was evaluated for developmental delay and tremor from the age of 17 months onwards. She has bilateral cataracts and chronic moderate neutropenia (0.6-0.9 G/L) but did not suffer recurrent infections beside *Salmonella* infection at 17 years of age. Hypothyroidism and hypergonadotropic hypogonadism were treated with hormonal substitution. She is now 18 years old and finished regular school with some support. Upon neurologic examination she shows normal head circumference, mild bilateral spasticity and severe cerebellar ataxia, dysarthria and tremor. She can walk with assistance and has no swallowing problems. MRI examination showed progressive, isolated, cerebellar atrophy **(Figure 1I).**

At the age of three months, muscular hypotonia, poor eye contact and uncoordinated eye movements were noted in the female **individual 7**. On eye examination a salt and pepper pigmentation pattern was observed, but no cataracts were observed. At the age of two years swallowing problems necessitated gastrostomy. From the age of four years seizures were noted. Eye-examination at that age was normal apart from strabismus (no cataract, no optic atrophy, no salt and pepper pigmentation). From the age of seven years onwards progressive athetosis and dystonia were noted as well as progressive spasticity of the legs. Serial MRI's up to the age of ten years showed progressive cerebral, cerebellar and basal ganglia atrophy and white matter involvement. An echocardiography at the age of 12 years revealed mild septal hypertrophy. Additionally, hypothyroidism was noted. **Individual 8** is the female cousin of individual 7 and shows an identical course of disease with additional epilepsy. Both individuals never showed neutropenia. The radiological findings of individual 8 are presented in **(Figure 1E-H).**

3. Severe phenotype (neutropenia, cataracts, infections, total lack of development, three individuals with fetal disease, early death and possible development of leukaemia)

Individual 9 was born prematurely at 35 weeks of gestation (wg) and pregnancy was complicated by IUGR. At birth severe generalized hypotonia, bilateral cataracts, a low nasal

bridge, hypertelorism and a tented mouth were noted **(Figure 1C).** She suffered severe drooling and recurrent airway infections as well as otitis media (e.g. pseudomonas aeroguinosa). Chronic severe neutropenia (0.0-0.4 G/L) was noted from the age of three months onwards. Her bone marrow showed maturation arrest at promyelocyte state **(Figure 2).** Continuous treatment with antibiotics, antimycotics and G-CSF as well as gastrostomy and extirpation of saliva glands helped stabilize her clinical condition. She displayed marked developmental delay, never learnt to roll over or to make contact. She had dystonic movements of the hands, feet and perioral and increasing muscle tone of the lower limbs and died at nearly four years of age due to increasing obstructive and central respiratory problems. Her MRI showed cerebellar hypoplasia (the vermis being more affected than the cortical hemispheres) and alterations in globus pallidus and capsula interna as well as white matter alterations in the parieto-occipital region. Evaluation of the oxidative phosphorylation system in fresh muscle and fibroblasts showed no abnormalities.

Individual 10 was born prematurely (35wg). Since birth he had sucking and swallowing difficulties and recurrent vomiting. At the age of 11 days he was hospitalized with clinical signs of sepsis. Since the second week of life severe neutropenia (<0.5 G/L), monocytosis, and recurrent bacterial infections were noticed. He needed tube feeding due to bulbar paralysis and absent swallowing reflexes. Dysmorphic features were noticed involving high and hairy forehead, hypertelorism, low nasal bridge, retrognathia, dysplastic ears, clinodactyly of the hands and hypospadias, partial T2-3 syndactyly **(Figure 1A).** He had absolute developmental arrest; made no eye or other contact. Brain MRI revealed generalized brain atrophy. At the age of two months hepatosplenomegaly, progressive granulocytopenia and monocytosis were noted, and acute myeloid leukemia (phenotype M5; acute monocytic) was diagnosed. The morphological investigation of bone marrow aspirate showed predominantly dysplastic monocytes and dysplastic granulopoiesis. The karyotype from bone marrow cells was 46,XY(95%)/45,XY,-21/45XY,-7. Chemotherapy was initiated, but after the second course the individual deceased at 3.5 months of age. Upon brain autopsy generalized atrophy and polygyria were noted. His younger sister, **individual 11,** was born normally at term and showed identical dysmorphic features, and an identical course of disease with jaundice and group B streptococcal septicemia at day 3 of life. The same dysmorphic features with her brother were noted **(Figure 1B).** She made no eye contact or showed any development. Brain MRI showed generalized brain atrophy and delayed myelination. She had very weak swallowing and sucking reflexes necessitating tube feeding. Furthermore, she suffered progressive severe neutropenia (<0.5 G/L), monocytosis (33-70%) and hepatomegaly from

birth onwards. Bone marrow morphological investigation and immuno-phenotyping was performed three times. There was a predominance of atypical dysplastic monocytes (33-74%), mature neutrophils were almost absent and 10-15% of blasts cells were present. Myelodysplastic syndrome and pre-leukaemic syndrome were diagnosed with a possibility of myelomonocytaric leukaemia. Following the wish of parents she received only palliative care and died at 3.5 months of age. No autopsy was performed.

Individual **12** had *in utero* complications including IUGR, decreased placental flow and polyhydramnion and manifested fetal oedema. From the first day of life, significantly increased muscle tension and jaw clenching were noticed ("stiff baby"). Massive limb tremor, generalized seizures resistant to anticonvulsants, and non-epileptic periodical apnea and unconsciousness were observed and persisted through life. Brain ultrasound, ocular fundus examination and neonatal hearing screening were normal. During the neonatal period the girl presented with increasing respiratory failure and feeding problems for which she received parenteral/tube feeding and transiently assisted ventilation. She had severe chronic neutropenia (0.1-0.7 10E9/l) and suffered severe bacterial and fungal infections despite treatment with antibiotics, antimycotics and G-CSF. Bone marrow biopsy showed vacuolar degeneration of the phagocytic mononuclear system (without typical signs of known congenital neutropenia). She showed hardly no development until passing away at five months of age due to an infection with consecutive cardiorespiratory failure. On autopsy microcephaly, marked loss of cellular structures in both hemispheres of the brain and a total depletion of cellular structures of the cerebellum and brainstem were reported.

The pregnancy with **individual 13** was complicated by placental calcifications, polyhydramnion and IUGR and ended at term by Caesarian section due to fetal distress. The newborn period was dominated by signs of respiratory failure, pneumonia and severe leukopenia. The individual presented tetraspasticity and forced flexion of the limbs, furthermore lockjaw (“stiff baby”), nystagmus and trembling of limbs. He died at months of age. The pregnancy of his younger brother, **individual 14,** was complicated by intrauterine jitteriness / seizures. From birth onwards the individual was jittery, unconscious, non reactive, made no contact and showed severe hypertonia (“stiff baby”). Echocardiographic examination revealed mild dilated cardiomyopathy. Head ultrasound showed abnormal brain structures, no details were reported. Additionally, from the 3rd week of life oliguria appeared followed by generalized oedema. Laboratory studies included persistent leukopenia reaching 1.2 G/L with lymphocythosis. Despite intensive medical treatment, the individual passed away at 24 days of age.

Supplemental figures and tables

Figure S1. Schematic representation of the *D. rerio clpb* locus.

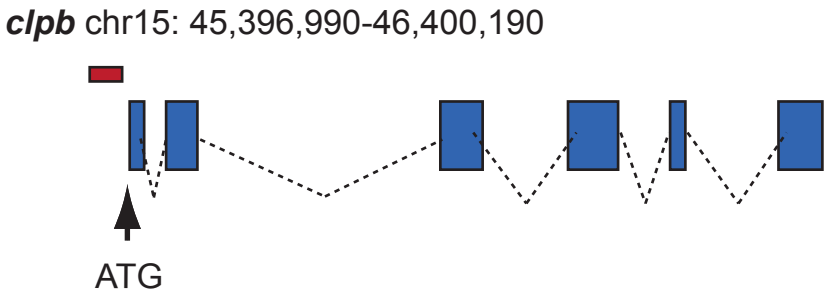

Blue, exons; dashed lines, introns; white, untranslated regions; red box, MO; ATG indicates the translation initiation site.

Figure S2. Preparations of CLPB protein and its p.Arg408Gly (p.R408G) variant.

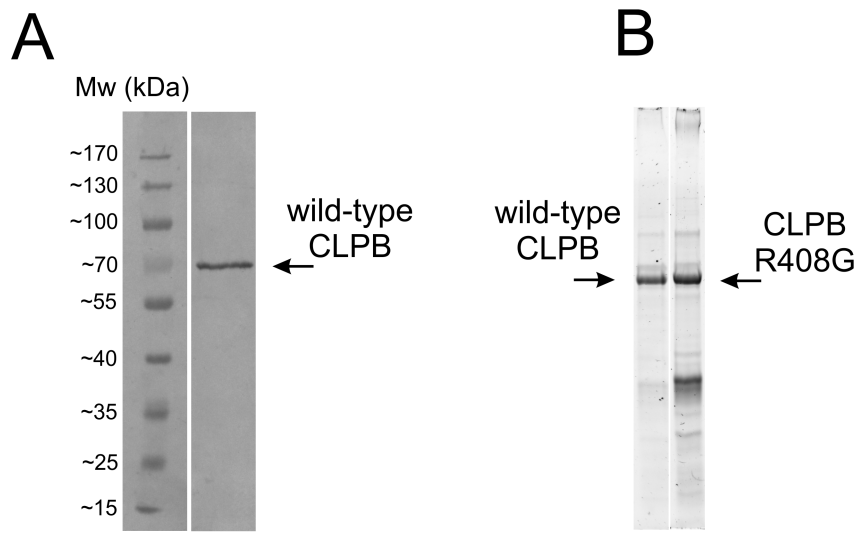

(A) Western blot of purified wild type CLPB protein with an anti-CLPB antibody (Abcam ab87253). B) SDS-PAGE of purified wild type and p.Arg408Gly CLPB sample (Biorad 12% TGX StainFree FastCast gel, visualised with Biorad ChemiDoc MP).

.

Figure S3. CLPB modeling.

Residues affected by missense mutations in the predicted CLPB protein structure (cyan). Two neighboring subunits (magenta and green) are shown, together with the position of the three subunits in the CLPB hexamer (insert). The structural model shown is based on *T. thermophilus* ClpB (pdb:1qvr) and prepared using and PyMOL (www.pymol.org) [20].

Figure S4. Conservation of the mutated CLPB amino acids in the individuals with *CLPB* mutations.

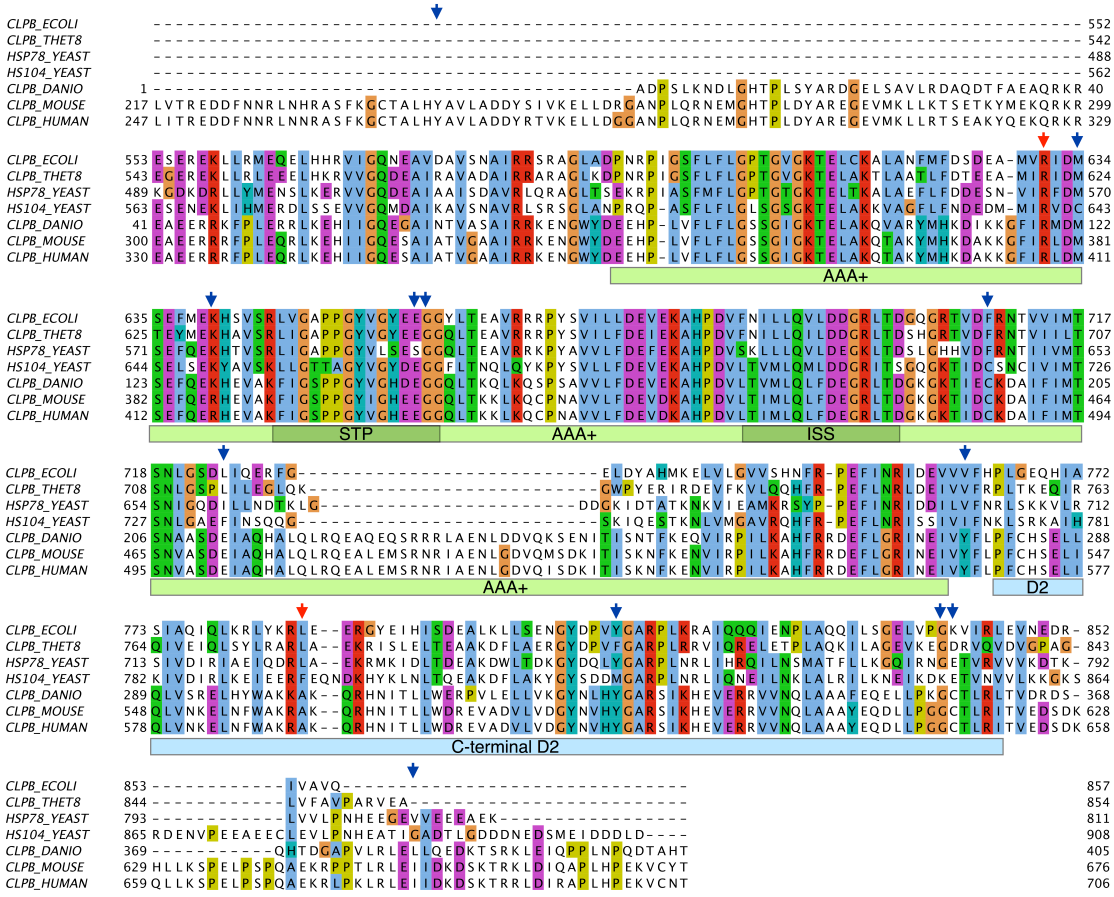

Alignment of the conserved region of human CLPB protein with its bacterial (*E. coli* and *T. thermophilus*), fungal (mitochondrial HSP78 and cytosolic HSP104) as well as vertebrate orthologs [zebrafish (*Danio rerio*) and mouse (*Mus musculus*)]. Arrows denote missense mutations in our cohort of individuals (blue: heterozygous, red: homozygous). Protein domains in the human sequence are marked under the alignment. AAA+ - ATPase domain, C-terminal D2 - CLPB-specific domain not present in other proteins from CLPA/C/X families. The C-terminal domain is essential for oligomerization, stabilizing the functional assembly [21; 22]. Structural motifs are highlighted in the alignment: STP - Substrate Translocation Pore (ISS - Inter-Subunit Signaling) motifs regulating ATP power-stroke for substrate translocation [23; 24]. The total length of the sequences is given in parentheses.

Figure S5. Expression of *CLPB* by mRNA expression analysis in human fetal and adult tissues.

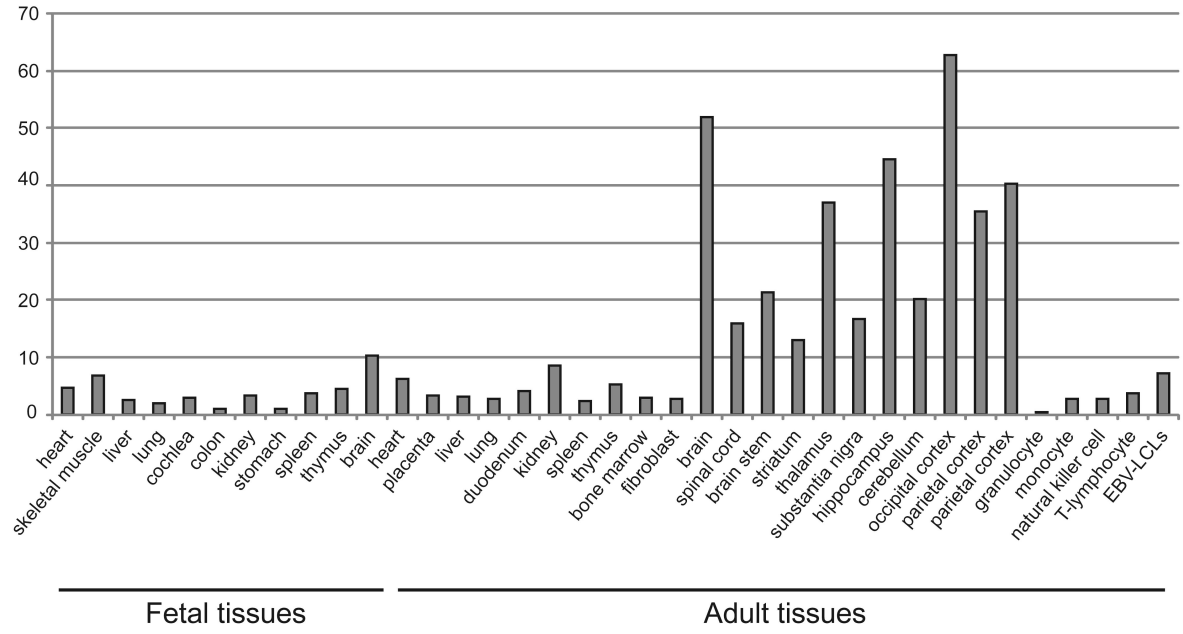

Total RNA from different human adult and fetal tissues was ordered from Stratagene Europe (Amsterdam, The Netherlands). All fetal tissues are from 20 or 21 week-old embryos after gestation, except for cochlear RNA that was isolated from an 8 week-old embryo by using the NucleoSpin RNA II kit (Macherey-Nagel, Düren, Germany) according to the manufacturer's protocols. To remove residual traces of genomic DNA, the cochlear RNA was treated with DNase I (Invitrogen, Leek, The Netherlands) while bound to the RNA binding column. Of all tissues, 5 µg of total RNA were transcribed into cDNA by using the iScript cDNA synthesis kit (Bio-Rad Laboratories, Hercules, CA, USA) according to the manufacturer's protocol. cDNA was purified by using the NucleoSpin extract II kit (Macherey-Nagel, Düren, Germany) according to the manufacturer's protocol. QPCR quantifications were performed in duplicate on the equivalent of 12.5 ng total RNA input. Experimental threshold cycles (Ct) values were within the range of cDNA dilutions used to validate the primers. The melt curves of all PCR products showed a single PCR product. All water controls were negative. GUSB (MIM #611499) and PPIB (MIM# 123841) were used as reference genes. Differences in expression between tissues were calculated by the comparative Ct or $2^{\Delta\Delta Ct}$ method [25; 26]. Relative expression levels are given as the fold change in comparison to the tissue with the lowest expression level.

Figure S6. Subcellular localization of CLPB.

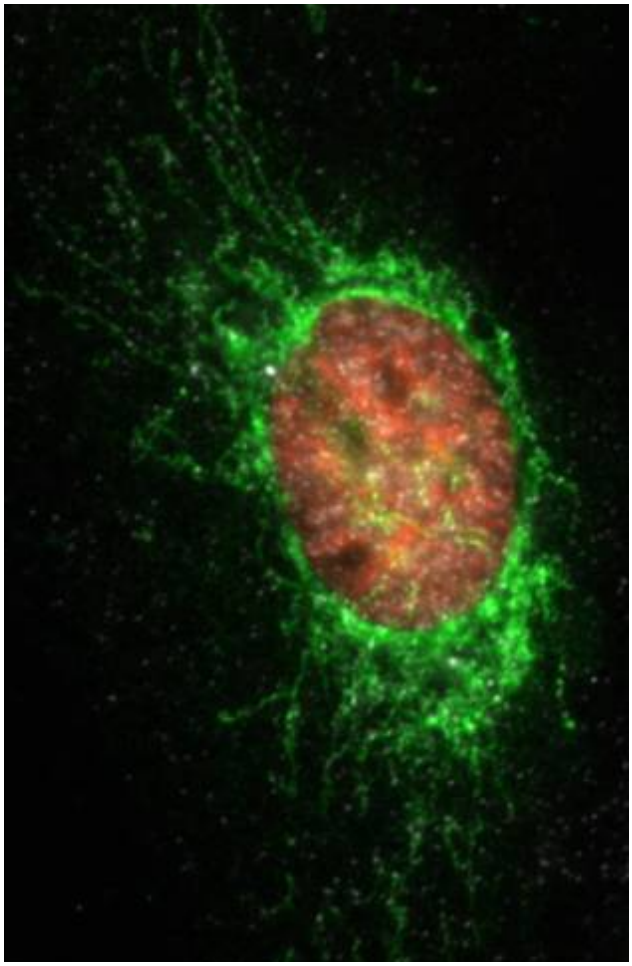

U2OS cells were transiently transfected with CLPB-V5 and pTagRFP-histone H2B expression constructs. CLPB-V5 (green) as well as HSP60 (white) were detected by immunofluorescence and showed mitochondrial co-localization distinct from the nuclear H2B fluorescence (red).

For immunofluorescent detection of V5 tagged CLPB, U2OS cells were grown on coverslips in six well plates and transiently transfected with a pLenti-CLPB-V5 expression construct using TransIT-LT1 (Mirus, Madison, WI) according the manufacturer's instructions. As a transfection efficiency control we co-transfected with a pTagRFP-H2B (Evrogen). The medium was replaced 4 hrs post-transfection with regular cell culture medium. Cells were fixed using 3.3% paraformaldehyde in cell culture medium for 15 min, washed 3x in PBS and permeabilized for 15 min with 0.5% Triton X100 in PBS/10% fetal calf serum (FCS). Primary V5 monoclonal antibody was diluted 1:100 and incubated in PBS/10%FCS for 1 hr. Secondary goat-anti-mouse IgG AlexaFluor 488 was likewise

incubated for 1 hr at a 1:1000 dilution. Slides were mounted using ProLong® Gold antifade with DAPI (Invitrogen). Image acquisition was performed using a Zeiss Observer.Z1with led illumination and appropriate emission filters.

Figure S7. Autophagy flux and mitochondrial clearance. (A, B, C)

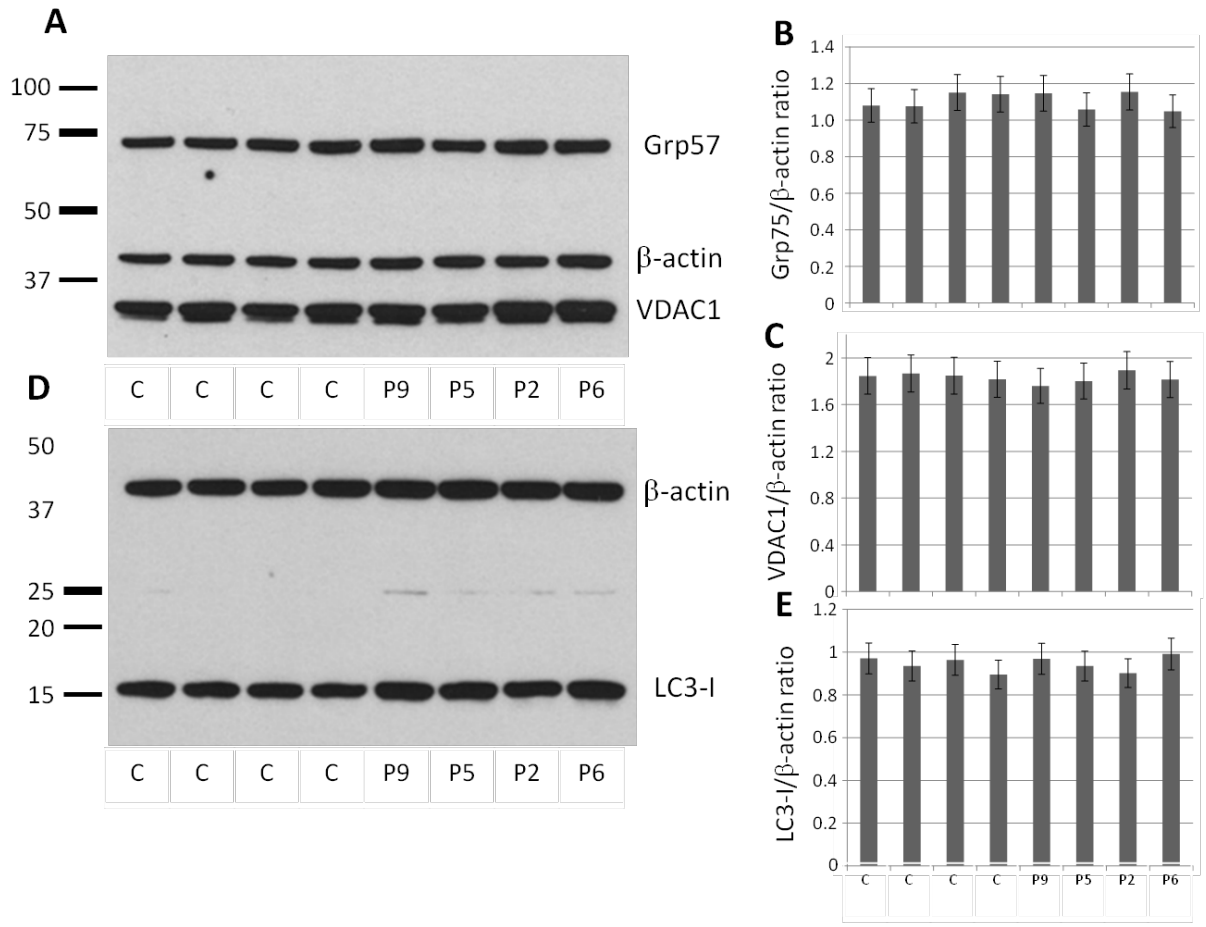

Mitochondrial clearance or mitophagy in fibroblasts under basal conditions was evaluated by measuring the mitochondrial proteins Grp75 and VDAC1 after immuno-blotting on SDS gels. β-Actin served as a loading control. Evidence for the presence or absence of mitophagy was based on the ratio of the two mitochondrial markers over β-actin in four individual cell lines (#9, 5, 2, 6) and four controls. No significant differences were observed. (D, E) Autophagy in fibroblasts was measured under basal conditions. We used the conversion of LC3 from its cytosolic form LC3-I (~17kDa) to the autophagy-relevant form LC3-II (~15kDa), a commonly used indicator of autophagy. The LC3 forms were separated on SDS gels and after immunoblotting expressed as ratio over β-actin using densitometry. No significant differences were found using four affected individual cell lines (#9, 5, 2 and 6) and 4 controls.

Fibroblasts that were used for assessment of mitophagy and autophagy, were kept in high glucose Dulbecco's Modified Eagle's Medium supplemented with 10% FCS (Lonza, Breda, The Netherlands) and 1% 10 U/µl Penicillin-10 µg/µl Streptomycin (Gibco, Breda, The Netherlands). All fibroblasts were grown at 5% CO2 and a temperature of 37°C.

In all assays, fibroblast passage numbers (<10) were matched. To challenge cellular processes of mitophagy by increasing the amount of dysfunctional mitochondria, fibroblasts were treated with the potassium ionophore valinomycin (1µM for 1h, Sigma-Aldrich, St. Louis, CA, USA). Proteins were extracted using RIPA buffer (50mM Tris-HCl pH7.6, 150mM NaCl, 1% DOC, 1% NP-40) containing 0.1% SDS. Cells were dissolved in the appropriate amount of buffer and incubated on ice for 30 min. Next, lysates were centrifuged at 16,000xg for 20min at 4oC. The supernatant was transferred into a new tube and used for Western blotting. Western blot analysis was performed as previously published using antibodies raised against β-actin (1:1000000, #A2228, Sigma-Aldrich, St. Louis, CA, USA), GRP75 (1:1000000, #ab2799, Abcam, Cambridge, UK), LC3 (1:1000, #4108, Cell Signaling Technology, Boston, MA, USA)[2].

Figure S8. Phospholipid analysis in fibroblasts of controls and individuals with the CLPB defect.

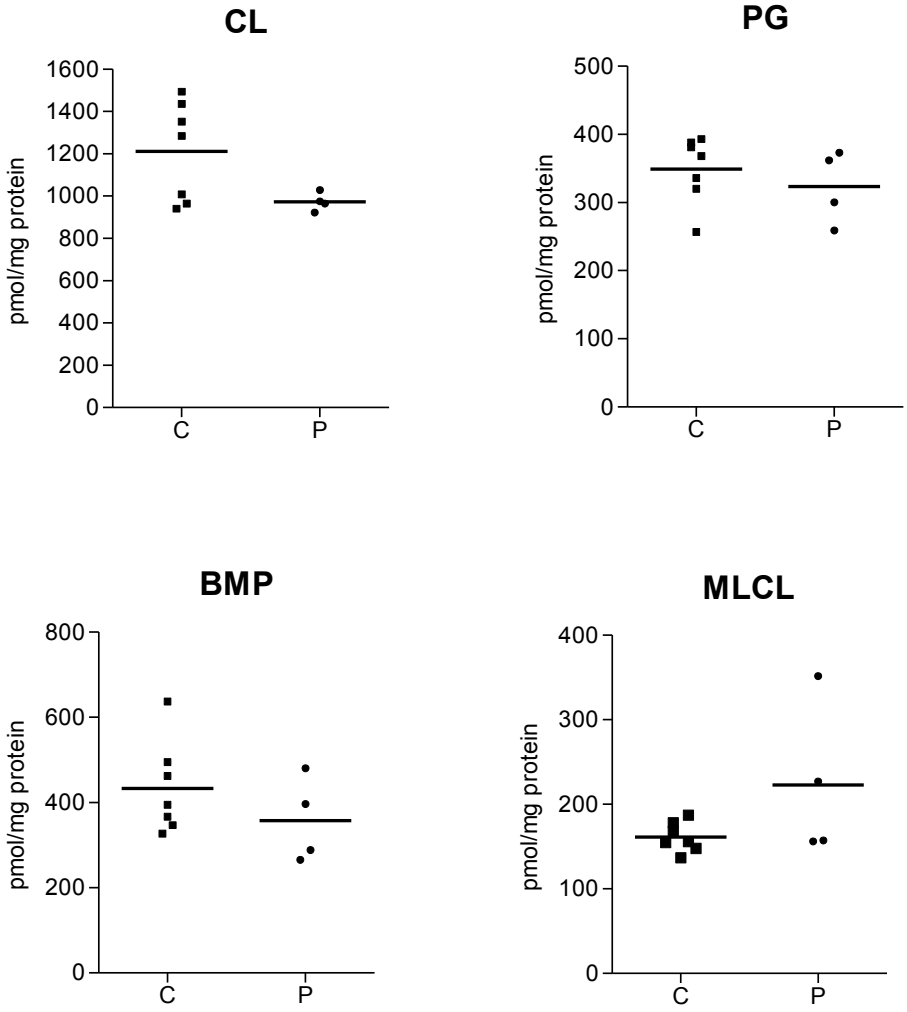

Scatter plots of the total levels of cardiolipin (CL), phosphatidylglycerol (PG), bis(monoacylglycerol)phosphate (BMP) and monolyso-cardiolipin (MLCL) in fibroblasts from controls ("C"; n=7) and affected individuals ("P"; n=4).

Statistical significance was assessed using a two-tailed student's t-test (CL (p=0.037), MLCL (p=0.273), PG (p=0.467) and BMP (p=0.283).

Fibroblast cell lines for phospholipid analysis were cultured in RPMI 1640 medium (Gibco, Breda, The Netherlands) containing 10% (v/v) fetal calf serum (FCS; Sigma, Zwijndrecht, The Netherlands), 1% 10 U/µl Penicillin-10 µg/µl Streptomycin (Gibco, Breda, The Netherlands), and 1% GlutaMAX (Gibco, Breda, The Netherlands). They were harvested by centrifugation at 200xg for 5 min at room temperature, washed once with PBS, pelleted by

centrifugation at 200xg for 5 min at room temperature, and snap frozen in liquid nitrogen. Levels of the following phospholipids were analyzed: PG, BMP, CL and phosphatidic acid (PA), phosphatidylcholine (PC), phosphatidylethanolamine (PE), phosphatidylserine (PS) phosphatidylinositol (PI), sphingomyeline (SM) and their lyso-analogue species. The relative abundances of the species in the sample-extracts were determined by HPLC-MS/MS using a Surveyor HPLC system hyphenated to a TSQ Quantum AM tandem mass spectrometer (Thermo Finnigan Corporation, San Jose, CA, USA). The MS was operated alternating in the negative- and positive ion electrospray ionization (ESI) mode in consecutive runs as described in detail previously [3]. Acyl-chain compositions were determined by the product-ion scans of the respective *quasi* molecular ions.

Figure S9. CNS disorganization upon translation blocking morpholino in the CLPB zebrafish model.

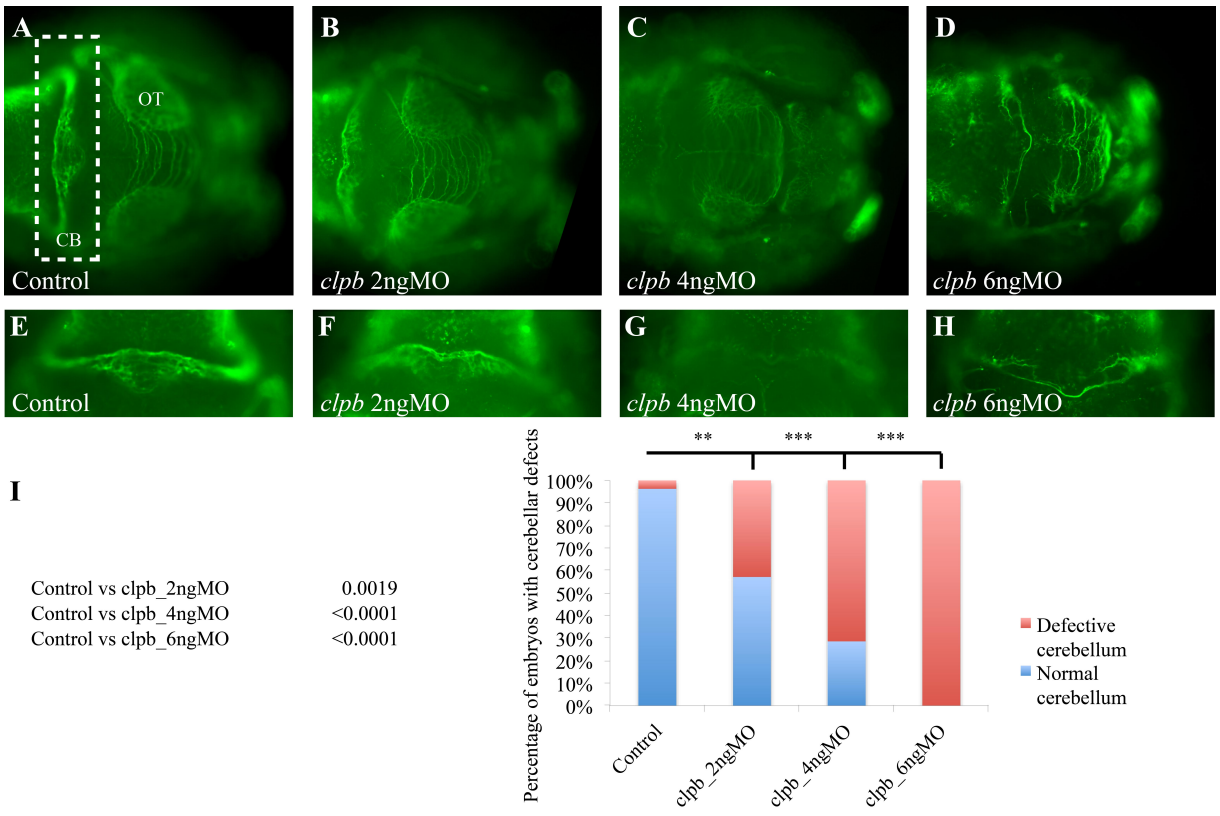

(A-D) Dorsal view of the brain stained with acetylated tubulin in 3 days post fertilization (dpf) in developing zebrafish embryos. A progressive disorganization of the CNS is observed with increasing doses of a translation-blocking morpholino (MO) against *clpb* (TB-*clpb*). More specifically, embryos injected with higher doses of MO show microcephaly, reduction of the size of the optic tectum (OT; a structure equivalent to the superior culliculus in humans), and degeneration of the axons forming the cerebellum (CB). (E-H). Magnifications of the cerebellum, highlighted with the white dashed line in panel A. (I) p-values and quantification of the embryos showing defects in the cerebellum across progressively increasing doses of MO.

Figure S10. Overexpression of the non-synonymous *CLPB* alleles tested with the *in vivo* functional model.

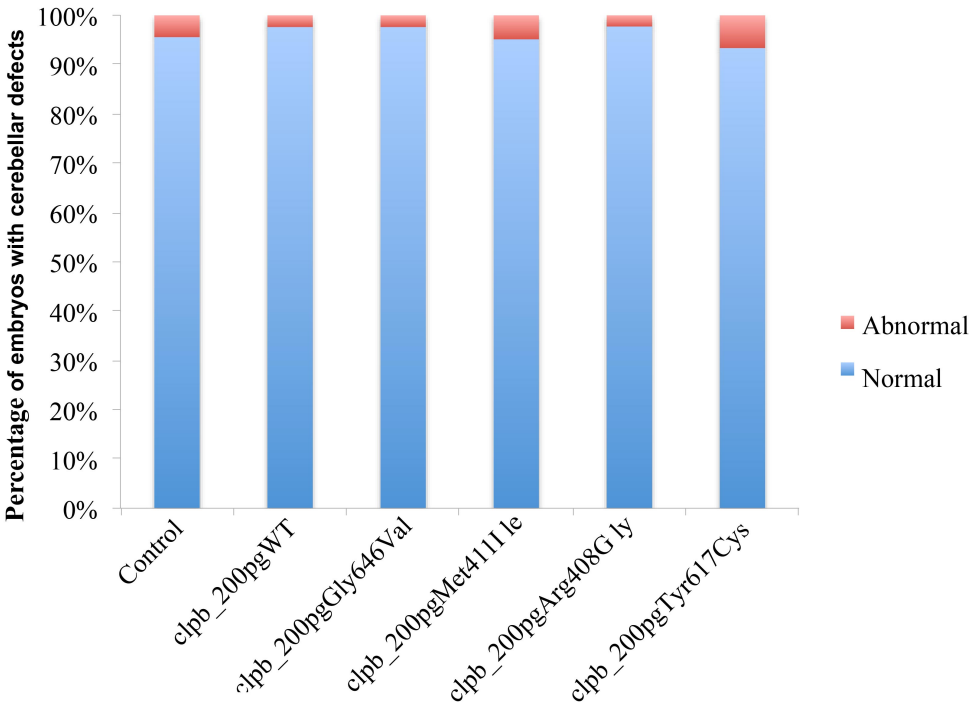

Overexpression of wt *CLPB* mRNA or *CLPB* mRNA harboring any of the variants identified in the study cohort (p.Arg408Gly, p.Met411Ile, p.Tyr617Cys and p.Gly646Val) does not lead to changes in the integrity of the cerebellum in zebrafish embryos at 72 hpf, suggesting that injection of each of the mutant constructs alone does not lead to toxicity and induction of a phenotype similar to the morpholino.

Figure S11. ATPase activity of purified wildtype and p.Arg408Gly (p.R408G) ClpB.

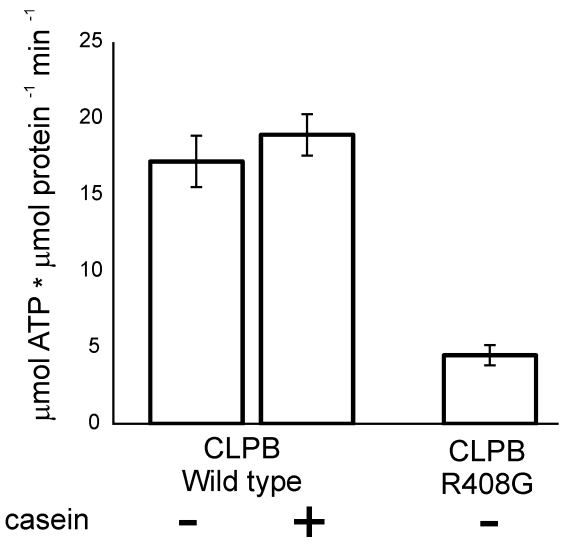

ATPase activity of purified wildtype and p.Arg408Gly (p.R408G) ClpB. All measurements were run in triplicate. Mutant ClpB had 26% ATPase activity compared to wild type human ClpB.

Table S1. Primer sequences for Sanger Sequencing of *CLPB* (NM_030813.4)

Exon	Forward primer (5'→3')	Reverse primer (5'→3')
1	caggaaacagctatgaccGGCAGCCATGTTGGACGTGG	tgtaaaacgacggccagtAGTTAGGACAATCTTCCCGCC
2	caggaaacagctatgaccGTACTGCCACTGTCTTAGTGG	tgtaaaacgacggccagtTCCAAAGCAAAGTCATCACACG
3	caggaaacagctatgaccCACACCAGGTGGGAGAGTGC	tgtaaaacgacggccagtCAGATGTCAAGCCATACACTG
4	caggaaacagctatgaccTCCGGATCTGGGTCTGTACC	tgtaaaacgacggccagtACAGAGGTAAAGAACATGCAGG
5	caggaaacagctatgaccTCTGGGGGTAGAGGGCTTGG	tgtaaaacgacggccagtAAAGAGATAGTCAGATGAGACC
6	caggaaacagctatgaccGGAGGATAACAGGGCTCTGG	tgtaaaacgacggccagtTGCCTCTTCTTACCCAGCAC
7	caggaaacagctatgaccGAAATCAGAGCCTTAAGCCACC	tgtaaaacgacggccagtAGTGAAGGATTAAATGATGCATGG
8	caggaaacagctatgaccCTATGAAGCAGGACCCCTGG	tgtaaaacgacggccagtATCCAGTTTGGTGACGACAGG
9	caggaaacagctatgaccATACTTAGTGATAATTATCCTGCC	tgtaaaacgacggccagtGGAGGCCGTTGCTTTTAGAGC
10	caggaaacagctatgaccTGCGCCTCAACATTCTCATCC	tgtaaaacgacggccagtTTCAGAGGGTCAGATTTTTTGGG
11	caggaaacagctatgaccGGGATAGTTGAGGTGCTCTCC	tgtaaaacgacggccagtTGAGGCCCAAATGACAAGACC
12	caggaaacagctatgaccTCTCTGTTGAGAGAGGCAACC	tgtaaaacgacggccagtGAATGACCAGCTAGCCTCTGG
13	caggaaacagctatgaccGGAGGTGAGAACTGAGAGTGC	tgtaaaacgacggccagtAGCTAGGGACAGAGCTGCCC
14	caggaaacagctatgaccTTTCCATGGGCAGGCCAAGG	tgtaaaacgacggccagtGGCTTCCAGATCTTTAGGATGG
15-16	caggaaacagctatgaccTGGTAATTTCCCTAACCCGC	tgtaaaacgacggccagtCAAGCTATAGGGAGGCAGGC
17	caggaaacagctatgaccGGTCTCTGAGTTGCCCTAGC	tgtaaaacgacggccagtAGGCCTGAGACTGGGTAGAG

Overview of the PCR primers used to amplify the exons of the *CLPB* gene (NM_030813.4). All primers contained a M13 sequence at the 5'end that allowed for sequencing of the PCR products using universal M13 primers.

Table S2. Primer sequences of primers used for QPCR analysis of *CLPB* (NM_030813.4)

	Forward primer (5'→3')	Reverse primer (5'→3')
GUSB (NM_000181.1)	agagtggtgctgaggattgg	ccctcatgctctagcgtgtc
PPIB (NM_000942.4)	cggaaagactgttccaaaaac	gattacacgatggaatttgctg
CLPB (NM_030813.4)	tgaataaagaaatgtaaagg	ttaataaattaaaattatag

Table S3. Oxidative phosphorylation measurements in muscle and cultured fibroblasts

	parameter	Individual 6	Individual 9	reference value	unit
muscle	ATP + CrP production rate	28,8	ND	15.4 - 30.2	nmol ATP.h^{-1}.(mU CS)$^{-1}$
	pyruvate oxidation rate	3,01	1,96	1.74 - 3.11	nmol CO_2.h^{-1}.(mU CS)$^{-1}$
	complex I	69	102	47 - 154	mU.(mU CS)-1
	complex II	247	230	134 - 354	mU.(mU CS)-1
	complex III	954	969	696 - 1756	mU.(mU CS)-1
	complex IV	1381	1189	470 - 1842	mU.(mU CS)-1
	complex V	358	349	161 - 711	mU.(mU COX)-1
	complex II+III	347	308	176 - 492	mU.(mU CS)-1
	citrate synthase	238	187	84 - 365	mU.(mg protein)-1
fibroblasts	complex I	342	318	163 - 599	mU.(mU CS)-1
	complex II	465	435	335 - 888	mU.(mU CS)-1
	complex III	850	694	570 - 1383	mU.(mU CS)-1
	complex IV	604	537	288 - 954	mU.(mU CS)-1
	complex V	711	635	193 - 819	mU.(mU CS)-1
	complex II+III	267	263	128 - 534	mU.(mU CS)-1
	citrate synthase	302	370	151 - 449	mU.(mg protein)-1

ND = not determined.

OXPHOS measurements in different tissues were performed as reported earlier. The measurement of the oxygen consumption rate in the presence of pyruvate and malate as mitochondrial respiration substrates was performed as described previously [1].

Table S4. Direct interaction partners of CLPB as identified by database searches.

	Database	Method	Reference
COPS6	STRING	Affinity Capture-MS	[9]
COPS6	BioGRID		
CUL3	BioGRID	Affinity Capture-MS	[10]
ERCC6L	BioGRID	Affinity Capture-MS	Huttlin EL (2014/pre-pub)
HDAC11	BioGRID	Affinity Capture-MS	[11]
IRS4	BioGRID	Affinity Capture-Luminescence	[12]
IRS4	BioGRID	Affinity Capture-MS	[12]
MDFI	IntAct	Two-hybrid	[13]
MDFI	BioGRID		
MGEA5	BioGRID	Affinity Capture-MS	*
OSBPL10	STRING	Affinity Capture-MS	[9]
SMAD9	HPRD	Two-hybrid	[14]
SMAD9	IntAct		
SMAD9	MINT		
TERF2	BioGRID	Affinity Capture-MS	[15]
TSEN2	BioGRID	Affinity Capture-MS	*
TTF2	HPRD	Affinity Capture-MS	*
TTF2	STRING	Two-hybrid	[16]
UBC	BioGRID	Affinity Capture-MS	[17]
UCHL3	STRING	Affinity Capture-MS	[9]
UCHL3	BioGRID	Affinity Capture-MS	*
USP30	STRING	Affinity Capture-MS	Sowa ME (2009)
USP30	BioGRID		
RG9MTD1	STRING	CoIP	[18]
STIP1	STRING	CoIP	[19]

* http://thebiogrid.org/166968/publication/high-throughput-proteomic-mapping-of-human-interaction-networks-via-affinity-purification-mass-spectrometry.html (Huttlin EL et al. High throughput proteomic mapping of human interaction networks via affinity-purification mass spectrometry (pre-publication)).Data on proteins that physically interact with CLPB (**Table S4**) were retrieved from public databases (BioGRID, Biological General Repository for Interaction Datasets; HPRD, Human Protein Reference Database; MINT, Molecular Interactions Database; STRING, Search Tool for the Retrieval of Interacting Genes/Proteins). Database information on physical protein interactions for HAX1 was obtained from the most recent release from the BioGRID database (www.thebiogrid.org/download.php; compiled on October 25th 2014).

In addition, a live cell protein interaction screen of CLPB against a library of *n* = 100 proteins was performed using bioluminescence resonance energy transfer (BRET), as described before[4; 5]. Briefly, we generated a protein library enriched for gene ontology (GO) tags linked to functions and processes that are associated with 3-MGA-uria[6; 7]. Proteins were selected from a library of n > 500 proteins based on the number of associations with GO biological_process (phospholipid biosynthetic process, cholesterol homeostasis, lipid metabolic process, response to calcium ion, calcium ion binding, membrane organization) and GO cellular_component (endoplasmic reticulum, mitochondrion, peroxisome, Golgi apparatus, integral to membrane).

Table S5. Proteins interacting with CLPB as determined by BRET.

#	Interaction partner	BRET pair		BRET Ratio	
	Name	*Protein 1*	*Protein 2*	*1st experiment*	*2nd experiment*
1	ABCD4	CLBP-C-Venus	ABCD4-C-hRluc	0,019	0.035 *
2	AGXT	CLBP-C-Venus	AGXT-C-hRluc	0.028 *	0.037 *
3	ATP2A2	CLBP-N-Venus	ATP2A2-N-hRluc	0.028 *	0,000
4	CARD8	CLBP-N-Venus	CARD8-N-hRluc	0.051 *	0.059 *
5	CYB5	CLBP-N-hRluc	CYB5-C-Venus	0,020	0.027 *
6	FAR1	CLBP-N-hRluc	FAR1-C-Venus	0,013	0.027 *
7	FASN	CLBP-N-hRluc	FASN-N-Venus	0,013	0.027 *
8	FIS1	CLBP-N-hRluc	FIS1-C-Venus	0.055 *	0.033 *
9	HMGCL	CLBP-C-Venus	HMGCL-C-hRluc	0,000	0.029 *
10	IL1B	CLBP-N-hRluc	IL1B-N-Venus	0.027 *	0,026
11	MIF	CLBP-N-hRluc	MIF-C-Venus	0.051 *	0,025
12	MPV17L2	CLBP-N-hRluc	PEX19-N-Venus	0.050 *	0.062 *
13	NLRP2	CLBP-N-hRluc	PEX5isob-N-Venus	0.056 *	0.054 *
14	PEX19	CLBP-N-hRluc	PYCARD-C-Venus	0.062 *	0.057 *
15	PEX5isob	CLBP-N-hRluc	RIPK2-N-Venus	0.030 *	0,025
16	PYCARD	CLBP-N-Venus	SSR1-C-hRluc	0,000	0.037 *
17	RIPK2	CLBP-N-Venus	MPV17L2-N-hRluc	0.037 *	0,000
18	SSR1	CLBP-N-hRluc	NLRP2-N-Venus	0.030 *	0,002
19	SERAC1	SERAC1-N-Venus	CLBP-N-hRluc	0.028 *	0.027 *

A live-cell screen of CLPB against a library of 100 proteins by means of bioluminescence resonance energy transfer (BRET) identified 19 positive interactions. The library of 100 proteins was derived from a random library by enrichment for proteins associated with the Gene Ontology (GO) annotations biological_processes phospholipid biosynthetic process, cholesterol homeostasis, lipid metabolic process, response to calcium ion, calcium ion binding, membrane organization, and GO cellular_components endoplasmic reticulum, mitochondrion, peroxisome, Golgi apparatus, integral to membrane. The protein interaction pairs are given and the orientation (C, C-terminus; N, N-terminus) of BRET tags (Venus, variant of yellow fluorescent protein; Rluc, Renilla luciferase) is indicated. Protein interactions were assumed as true positive, if the BRET ratio of at least one experiment exceeded a method specific threshold of 0.0263 (indicated by *).

BRET protein-protein interaction assays were performed in transfected COS-7 cells as described before[4; 5]. Full-length open reading frames of genes encoding CLPB (BC 006404.2) and genes encoding proteins of the $n = 100$ library were introduced into plasmid vectors for

the expression of amino- and carboxy-terminal fusions with Rluc or YFP. All eight possible combinations of Rluc (donor) or YFP (acceptor) fusions tagged at the amino or carboxyl terminus were tested in duplicates for each putative interaction pair at an acceptor/donor ratio of 3:1. BRET ratios were calculated by the equation $R = (I_A / I_D) - cf$, where R is the BRET ratio, I_A is the BRET signal, I_D is the Rluc signal and cf is a correction factor ($(I_A / I_D)_{control}$), with co-transfection of the donor fusion protein with YFP in the absence of the second protein of interest used as the control. Protein interactions were assumed to be true positive, if the BRET ratio of at least one combination of acceptor and donor tagged interaction pairs exceeded a method-specific threshold of 0.0263. The threshold for classification of positive protein interactions was generated by measurement of two libraries of $n = 60$ proteins with known positive protein interactions (positive reference set, PRS) and putatively negative protein interactions (random reference set, RRS), as described previously [8].

References

1. Rodenburg, R.J. (2011). Biochemical diagnosis of mitochondrial disorders. Journal of inherited metabolic disease 34, 283-292.
2. Rakovic, A., Grunewald, A., Kottwitz, J., Bruggemann, N., Pramstaller, P.P., Lohmann, K., and Klein, C. (2011). Mutations in PINK1 and Parkin impair ubiquitination of Mitofusins in human fibroblasts. PloS one 6, e16746.
3. Houtkooper, R.H., Rodenburg, R.J., Thiels, C., van Lenthe, H., Stet, F., Poll-The, B.T., Stone, J.E., Steward, C.G., Wanders, R.J., Smeitink, J., et al. (2009). Cardiolipin and monolysocardiolipin analysis in fibroblasts, lymphocytes, and tissues using high-performance liquid chromatography-mass spectrometry as a diagnostic test for Barth syndrome. Analytical biochemistry 387, 230-237.
4. Bakele, M., Lotz-Havla, A.S., Jakowetz, A., Carevic, M., Marco, V., Munta, A.C., Gerstin, S.W., and Hartl, D. (2014). An interactive network of elastase, secretases, and PAR-2 protein regulates CXCR1 receptor surface expression on neutrophils. The Journal of biological chemistry 289, 20516-20525.
5. Gersting, S.W., Lotz-Havla, A.S., and Muntau, A.C. (2012). Bioluminescence resonance energy transfer: an emerging tool for the detection of protein-protein interaction in living cells. Methods in molecular biology (Clifton, NJ) 815, 253-263.
6. Wortmann, S.B., Duran, M., Anikster, Y., Barth, P.G., Sperl, W., Zschocke, J., Morava, E., and Wevers, R.A. (2013). Inborn errors of metabolism with 3-methylglutaconic aciduria as discriminative feature: proper classification and nomenclature. Journal of inherited metabolic disease 36, 923-928.
7. Wortmann, S.B., Espeel, M., Almeida, L., Reimer, A., Bosboom, D., Roels, F., de Brouwer, A.P., and Wevers, R.A. (2014). Inborn errors of metabolism in the biosynthesis and remodelling of phospholipids. Journal of inherited metabolic disease.
8. Braun, P., Tasan, M., Dreze, M., Barrios-Rodiles, M., Lemmens, I., Yu, H., Sahalie, J.M., Murray, R.R., Roncari, L., de Smet, A.S., et al. (2009). An experimentally derived confidence score for binary protein-protein interactions. Nature methods 6, 91-97.
9. Sowa, M.E., Bennett, E.J., Gygi, S.P., and Harper, J.W. (2009). Defining the human deubiquitinating enzyme interaction landscape. Cell 138, 389-403.
10. Bennett, E.J., Rush, J., Gygi, S.P., and Harper, J.W. (2010). Dynamics of cullin-RING ubiquitin ligase network revealed by systematic quantitative proteomics. Cell 143, 951-965.
11. Joshi, P., Greco, T.M., Guise, A.J., Luo, Y., Yu, F., Nesvizhskii, A.I., and Cristea, I.M. (2013). The functional interactome landscape of the human histone deacetylase family. Molecular systems biology 9, 672.
12. Taipale, M., Tucker, G., Peng, J., Krykbaeva, I., Lin, Z.Y., Larsen, B., Choi, H., Berger, B., Gingras, A.C., and Lindquist, S. (2014). A quantitative chaperone interaction network reveals the architecture of cellular protein homeostasis pathways. Cell 158, 434-448.
13. Venkatesan, K., Rual, J.F., Vazquez, A., Stelzl, U., Lemmens, I., Hirozane-Kishikawa, T., Hao, T., Zenkner, M., Xin, X., Goh, K.I., et al. (2009). An empirical framework for binary interactome mapping. Nature methods 6, 83-90.
14. Colland, F., Jacq, X., Trouplin, V., Mougin, C., Groizeleau, C., Hamburger, A., Meil, A., Wojcik, J., Legrain, P., and Gauthier, J.M. (2004). Functional proteomics mapping of a human signaling pathway. Genome research 14, 1324-1332.
15. Giannone, R.J., McDonald, H.W., Hurst, G.B., Shen, R.F., Wang, Y., and Liu, Y. (2010). The protein network surrounding the human telomere repeat binding factors TRF1, TRF2, and POT1. PloS one 5, e12407.
16. Leonard, D., Ajuh, P., Lamond, A.I., and Legerski, R.J. (2003). hLodestar/HuF2 interacts with CDC5L and is involved in pre-mRNA splicing. Biochemical and biophysical research communications 308, 793-801.
17. Stes, E., Laga, M., Walton, A., Samyn, N., Timmerman, E., De Smet, I., Goormachtig, S., and Gevaert, K. (2014). A COFRADIC protocol to study protein ubiquitination. Journal of proteome research 13, 3107-3113.

18. Holzmann, J., Frank, P., Loffler, E., Bennett, K.L., Gerner, C., and Rossmanith, W. (2008). RNase P without RNA: identification and functional reconstitution of the human mitochondrial tRNA processing enzyme. Cell 135, 462-474.
19. Behrends, C., Sowa, M.E., Gygi, S.P., and Harper, J.W. (2010). Network organization of the human autophagy system. Nature 466, 68-76.
20. Biasini, M., Bienert, S., Waterhouse, A., Arnold, K., Studer, G., Schmidt, T., Kiefer, F., Cassarino, T.G., Bertoni, M., Bordoli, L., et al. (2014). SWISS-MODEL: modelling protein tertiary and quaternary structure using evolutionary information. Nucleic acids research 42, W252-258.
21. Lee, S., Sowa, M.E., Watanabe, Y.H., Sigler, P.B., Chiu, W., Yoshida, M., and Tsai, F.T. (2003). The structure of ClpB: a molecular chaperone that rescues proteins from an aggregated state. Cell 115, 229-240.
22. Mogk, A., Schlieker, C., Strub, C., Rist, W., Weibezahn, J., and Bukau, B. (2003). Roles of individual domains and conserved motifs of the AAA+ chaperone ClpB in oligomerization, ATP hydrolysis, and chaperone activity. The Journal of biological chemistry 278, 17615-17624.
23. Leidhold, C., von Janowsky, B., Becker, D., Bender, T., and Voos, W. (2006). Structure and function of Hsp78, the mitochondrial ClpB homolog. Journal of structural biology 156, 149-164.
24. Biter, A.B., Lee, S., Sung, N., and Tsai, F.T. (2012). Structural basis for intersubunit signaling in a protein disaggregating machine. Proceedings of the National Academy of Sciences of the United States of America 109, 12515-12520.
25. Pfaffl, M.W. (2001). A new mathematical model for relative quantification in real-time RT-PCR. Nucleic acids research 29, e45.
26. Livak, K.J., and Schmittgen, T.D. (2001). Analysis of relative gene expression data using real-time quantitative PCR and the 2(-Delta Delta C(T)) Method. Methods (San Diego, Calif) 25, 402-408.